

Open Charm Yields in $d + \text{Au}$ Collisions at $\sqrt{s_{NN}} = 200 \text{ GeV}$

J. Adams,³ M. M. Aggarwal,²⁹ Z. Ahammed,⁴³ J. Amonett,²⁰ B. D. Anderson,²⁰ D. Arkhipkin,¹³ G. S. Averichev,¹² S. K. Badyal,¹⁹ Y. Bai,²⁷ J. Balewski,¹⁷ O. Barannikova,³² L. S. Barnby,³ J. Baudot,¹⁸ S. Bekele,²⁸ V. V. Belaga,¹² R. Bellwied,⁴⁶ J. Berger,¹⁴ B. I. Bezverkhny,⁴⁸ S. Bharadwaj,³³ A. Bhasin,¹⁹ A. K. Bhati,²⁹ V. S. Bhatia,²⁹ H. Bichsel,⁴⁵ A. Billmeier,⁴⁶ L. C. Bland,⁴ C. O. Blyth,³ B. E. Bonner,³⁴ M. Botje,²⁷ A. Boucham,³⁸ A. V. Brandin,²⁵ A. Bravar,⁴ M. Bystersky,¹¹ R. V. Cadman,¹ X. Z. Cai,³⁷ H. Caines,⁴⁸ M. Calderón de la Barca Sánchez,¹⁷ J. Castillo,²¹ D. Cebra,⁷ Z. Chajecski,⁴⁴ P. Chaloupka,¹¹ S. Chattopadhyay,⁴³ H. F. Chen,³⁶ Y. Chen,⁸ J. Cheng,⁴¹ M. Cherney,¹⁰ A. Chikanian,⁴⁸ W. Christie,⁴ J. P. Coffin,¹⁸ T. M. Cormier,⁴⁶ J. G. Cramer,⁴⁵ H. J. Crawford,⁶ D. Das,⁴³ S. Das,⁴³ M. M. de Moura,³⁵ A. A. Derevschikov,³¹ L. Didenko,⁴ T. Dietel,¹⁴ S. M. Dogra,¹⁹ W. J. Dong,⁸ X. Dong,³⁶ J. E. Draper,⁷ F. Du,⁴⁸ A. K. Dubey,¹⁵ V. B. Dunin,¹² J. C. Dunlop,⁴ M. R. Dutta Mazumdar,⁴³ V. Eckardt,²³ W. R. Edwards,²¹ L. G. Efimov,¹² V. Emelianov,²⁵ J. Engelage,⁶ G. Eppley,³⁴ B. Erazmus,³⁸ M. Estienne,³⁸ P. Fachini,⁴ J. Faivre,¹⁸ R. Fatemi,¹⁷ J. Fedorisin,¹² K. Filimonov,²¹ P. Filip,¹¹ E. Finch,⁴⁸ V. Fine,⁴ Y. Fisyak,⁴ K. Fomenko,¹² J. Fu,⁴¹ C. A. Gagliardi,³⁹ L. Gaillard,³ J. Gans,⁴⁸ M. S. Ganti,⁴³ L. Gaudichet,³⁸ F. Geurts,³⁴ V. Ghazikhanian,⁸ P. Ghosh,⁴³ J. E. Gonzalez,⁸ O. Grachov,⁴⁶ O. Grebenyuk,²⁷ D. Grosnick,⁴² S. M. Guertin,⁸ Y. Guo,⁴⁶ A. Gupta,¹⁹ T. D. Gutierrez,⁷ T. J. Hallman,⁴ A. Hamed,⁴⁶ D. Hardtke,²¹ J. W. Harris,⁴⁸ M. Heinz,² T. W. Henry,³⁹ S. Hepplemann,³⁰ B. Hippolyte,¹⁸ A. Hirsch,³² E. Hjort,²¹ G. W. Hoffmann,⁴⁰ H. Z. Huang,⁸ S. L. Huang,³⁶ E. W. Hughes,⁵ T. J. Humanic,²⁸ G. Igo,⁸ A. Ishihara,⁴⁰ P. Jacobs,²¹ W. W. Jacobs,¹⁷ M. Janik,⁴⁴ H. Jiang,⁸ P. G. Jones,³ E. G. Judd,⁶ S. Kabana,² K. Kang,⁴¹ M. Kaplan,⁹ D. Keane,²⁰ V. Yu. Khodyrev,³¹ J. Kiryluk,²² A. Kisiel,⁴⁴ E. M. Kislov,¹² J. Klay,²¹ S. R. Klein,²¹ D. D. Koetke,⁴² T. Kollegger,¹⁴ M. Kopytine,²⁰ L. Kotchenda,²⁵ M. Kramer,²⁶ P. Kravtsov,²⁵ V. I. Kravtsov,³¹ K. Krueger,¹ C. Kuhn,¹⁸ A. I. Kulikov,¹² A. Kumar,²⁹ R. Kh. Kutuev,¹³ A. A. Kuznetsov,¹² M. A. C. Lamont,⁴⁸ J. M. Landgraf,⁴ S. Lange,¹⁴ F. Laue,⁴ J. Lauret,⁴ A. Lebedev,⁴ R. Lednicky,¹² S. Lehocka,¹² M. J. LeVine,⁴ C. Li,³⁶ Q. Li,⁴⁶ Y. Li,⁴¹ G. Lin,⁴⁸ S. J. Lindenbaum,²⁶ M. A. Lisa,²⁸ F. Liu,⁴⁷ L. Liu,⁴⁷ Q. J. Liu,⁴⁵ Z. Liu,⁴⁷ T. Ljubicic,⁴ W. J. Llope,³⁴ H. Long,⁸ R. S. Longacre,⁴ M. Lopez-Noriega,²⁸ W. A. Love,⁴ Y. Lu,⁴⁷ T. Ludlam,⁴ D. Lynn,⁴ G. L. Ma,³⁷ J. G. Ma,⁸ Y. G. Ma,³⁷ D. Magestro,²⁸ S. Mahajan,¹⁹ D. P. Mahapatra,¹⁵ R. Majka,⁴⁸ L. K. Mangotra,¹⁹ R. Manweiler,⁴² S. Margetis,²⁰ C. Markert,²⁰ L. Martin,³⁸ J. N. Marx,²¹ H. S. Matis,²¹ Yu. A. Matulenko,³¹ C. J. McClain,¹ T. S. McShane,¹⁰ F. Meissner,²¹ Yu. Melnick,³¹ A. Meschanin,³¹ M. L. Miller,²² N. G. Minaev,³¹ C. Mironov,²⁰ A. Mischke,²⁷ D. K. Mishra,¹⁵ J. Mitchell,³⁴ B. Mohanty,⁴³ L. Molnar,³² C. F. Moore,⁴⁰ D. A. Morozov,³¹ M. G. Munhoz,³⁵ B. K. Nandi,⁴³ S. K. Nayak,¹⁹ T. K. Nayak,⁴³ J. M. Nelson,³ P. K. Netrakanti,⁴³ V. A. Nikitin,¹³ L. V. Nogach,³¹ S. B. Nurushev,³¹ G. Odyniec,²¹ A. Ogawa,⁴ V. Okorokov,²⁵ M. Oldenburg,²¹ D. Olson,²¹ S. K. Pal,⁴³ Y. Panebratsev,¹² S. Y. Panitkin,⁴ A. I. Pavlinov,⁴⁶ T. Pawlak,⁴⁴ T. Peitzmann,²⁷ V. Perevoztchikov,⁴ C. Perkins,⁶ W. Peryt,⁴⁴ V. A. Petrov,¹³ S. C. Phatak,¹⁵ R. Picha,⁷ M. Planinic,⁴⁹ J. Pluta,⁴⁴ N. Porile,³² J. Porter,⁴⁵ A. M. Poskanzer,²¹ M. Potekhin,⁴ E. Potrebenikova,¹² B. V. K. S. Potukuchi,¹⁹ D. Prindle,⁴⁵ C. Pruneau,⁴⁶ J. Putschke,²³ G. Rakness,³⁰ R. Raniwala,³³ S. Raniwala,³³ O. Ravel,³⁸ R. L. Ray,⁴⁰ S. V. Razin,¹² D. Reichhold,³² J. G. Reid,⁴⁵ G. Renault,³⁸ F. Retiere,²¹ A. Ridiger,²⁵ H. G. Ritter,²¹ J. B. Roberts,³⁴ O. V. Rogachevskiy,¹² J. L. Romero,⁷ A. Rose,⁴⁶ C. Roy,³⁸ L. Ruan,³⁶ R. Sahoo,¹⁵ I. Sakrejda,²¹ S. Salur,⁴⁸ J. Sandweiss,⁴⁸ M. Sarsour,¹⁷ I. Savin,¹³ P. S. Sazhin,¹² J. Schambach,⁴⁰ R. P. Scharenberg,³² N. Schmitz,²³ K. Schweda,²¹ J. Seger,¹⁰ P. Seyboth,²³ E. Shahaliev,¹² M. Shao,³⁶ W. Shao,⁵ M. Sharma,²⁹ W. Q. Shen,³⁷ K. E. Shestermanov,³¹ S. S. Shimanskiy,¹² E. Sichtermann,²¹ F. Simon,²³ R. N. Singaraju,⁴³ G. Skoro,¹² N. Smirnov,⁴⁸ R. Snellings,²⁷ G. Sood,⁴² P. Sorensen,²¹ J. Sowinski,¹⁷ J. Speltz,¹⁸ H. M. Spinka,¹ B. Srivastava,³² A. Stadnik,¹² T. D. S. Stanislaus,⁴² R. Stock,¹⁴ A. Stolpovsky,⁴⁶ M. Strikhanov,²⁵ B. Stringfellow,³² A. A. P. Suaide,³⁵ E. Sugarbaker,²⁸ C. Suire,⁴ M. Sumbera,¹¹ B. Sorrow,²² T. J. M. Symons,²¹ A. Szanto de Toledo,³⁵ P. Szarwas,⁴⁴ A. Tai,⁸ J. Takahashi,³⁵ A. H. Tang,²⁷ T. Tarnowsky,³² D. Thein,⁸ J. H. Thomas,²¹ S. Timoshenko,²⁵ M. Tokarev,¹² T. A. Trainor,⁴⁵ S. Trentalange,⁸ R. E. Tribble,³⁹ O. D. Tsai,⁸ J. Ulery,³² T. Ullrich,⁴ D. G. Underwood,¹ A. Urkinbaev,¹² G. Van Buren,⁴ M. van Leeuwen,²¹ A. M. Vander Molen,²⁴ R. Varma,¹⁶ I. M. Vasilevski,¹³ A. N. Vasiliev,³¹ R. Vernet,¹⁸ S. E. Vigdor,¹⁷ Y. P. Vijoyi,⁴³ S. Vokal,¹² S. A. Voloshin,⁴⁶ M. Vznuzdaev,²⁵ W. T. Waggoner,¹⁰ F. Wang,³² G. Wang,²⁰ G. Wang,⁵ X. L. Wang,³⁶ Y. Wang,⁴⁰ Y. Wang,⁴¹ Z. M. Wang,³⁶ H. Ward,⁴⁰ J. W. Watson,²⁰ J. C. Webb,¹⁷ R. Wells,²⁸ G. D. Westfall,²⁴ A. Wetzler,²¹ C. Whitten, Jr.,⁸ H. Wieman,²¹ S. W. Wissink,¹⁷ R. Witt,² J. Wood,⁸ J. Wu,³⁶ N. Xu,²¹ Z. Xu,⁴ Z. Z. Xu,³⁶ E. Yamamoto,²¹ P. Yepes,³⁴ V. I. Yurevich,¹² Y. V. Zanevsky,¹² H. Zhang,⁴ W. M. Zhang,²⁰ Z. P. Zhang,³⁶ R. Zoulkarneev,¹³ Y. Zoulkarneeva,¹³ and A. N. Zubarev¹²

(STAR Collaboration)

- ¹Argonne National Laboratory, Argonne, Illinois 60439, USA
²University of Bern, 3012 Bern, Switzerland
³University of Birmingham, Birmingham, United Kingdom
⁴Brookhaven National Laboratory, Upton, New York 11973, USA
⁵California Institute of Technology, Pasadena, California 91125, USA
⁶University of California, Berkeley, California 94720, USA
⁷University of California, Davis, California 95616, USA
⁸University of California, Los Angeles, California 90095, USA
⁹Carnegie Mellon University, Pittsburgh, Pennsylvania 15213, USA
¹⁰Creighton University, Omaha, Nebraska 68178, USA
¹¹Nuclear Physics Institute AS CR, 250 68 Řež/Prague, Czech Republic
¹²Laboratory for High Energy (JINR), Dubna, Russia
¹³Particle Physics Laboratory (JINR), Dubna, Russia
¹⁴University of Frankfurt, Frankfurt, Germany
¹⁵Institute of Physics, Bhubaneswar 751005, India
¹⁶Indian Institute of Technology, Mumbai, India
¹⁷Indiana University, Bloomington, Indiana 47408, USA
¹⁸Institut de Recherches Subatomiques, Strasbourg, France
¹⁹University of Jammu, Jammu 180001, India
²⁰Kent State University, Kent, Ohio 44242, USA
²¹Lawrence Berkeley National Laboratory, Berkeley, California 94720, USA
²²Massachusetts Institute of Technology, Cambridge, Massachusetts 02139-4307, USA
²³Max-Planck-Institut für Physik, Munich, Germany
²⁴Michigan State University, East Lansing, Michigan 48824, USA
²⁵Moscow Engineering Physics Institute, Moscow, Russia
²⁶City College of New York, New York, New York 10031, USA
²⁷NIKHEF, Amsterdam, The Netherlands
²⁸Ohio State University, Columbus, Ohio 43210, USA
²⁹Panjab University, Chandigarh 160014, India
³⁰Pennsylvania State University, University Park, Pennsylvania 16802, USA
³¹Institute of High Energy Physics, Protvino, Russia
³²Purdue University, West Lafayette, Indiana 47907, USA
³³University of Rajasthan, Jaipur 302004, India
³⁴Rice University, Houston, Texas 77251, USA
³⁵Universidade de Sao Paulo, Sao Paulo, Brazil
³⁶University of Science & Technology of China, Anhui 230027, China
³⁷Shanghai Institute of Applied Physics, Shanghai 201800, China
³⁸SUBATECH, Nantes, France
³⁹Texas A&M University, College Station, Texas 77843, USA
⁴⁰University of Texas, Austin, Texas 78712, USA
⁴¹Tsinghua University, Beijing 100084, China
⁴²Valparaiso University, Valparaiso, Indiana 46383, USA
⁴³Variable Energy Cyclotron Centre, Kolkata 700064, India
⁴⁴Warsaw University of Technology, Warsaw, Poland
⁴⁵University of Washington, Seattle, Washington 98195, USA
⁴⁶Wayne State University, Detroit, Michigan 48201, USA
⁴⁷Institute of Particle Physics, CCNU (HZNU), Wuhan 430079, China
⁴⁸Yale University, New Haven, Connecticut 06520, USA
⁴⁹University of Zagreb, Zagreb, HR-10002, Croatia

(Received 6 July 2004; published 17 February 2005)

Midrapidity open charm spectra from direct reconstruction of $D^0(\bar{D}^0) \rightarrow K^\pm \pi^\pm$ in $d + \text{Au}$ collisions and indirect electron-positron measurements via charm semileptonic decays in $p + p$ and $d + \text{Au}$ collisions at $\sqrt{s_{NN}} = 200$ GeV are reported. The $D^0(\bar{D}^0)$ spectrum covers a transverse momentum (p_T) range of $0.1 < p_T < 3$ GeV/c, whereas the electron spectra cover a range of $1 < p_T < 4$ GeV/c. The electron spectra show approximate binary collision scaling between $p + p$ and $d + \text{Au}$ collisions. From these two independent analyses, the differential cross section per nucleon-nucleon binary interaction at midrapidity for open charm production from $d + \text{Au}$ collisions at BNL RHIC is $d\sigma_{cc}^{NN}/dy = 0.30 \pm 0.04(\text{stat}) \pm 0.09(\text{syst})$ mb. The results are compared to theoretical calculations. Implications for charmonium results in $A + A$ collisions are discussed.

DOI: 10.1103/PhysRevLett.94.062301

PACS numbers: 25.75.Dw, 13.20.Fc, 13.25.Ft, 24.85.+p

Hadrons with heavy-flavor are unique tools for studying the strong interaction described by quantum chromodynamics (QCD). Because of the large mass of the charm quark ($\sim 1.5 \text{ GeV}/c^2$), charm quark production can be evaluated by perturbative QCD (PQCD) even at low momentum through the introduction of additional scales related to the charm quark mass [1,2]. Therefore, a theoretical calculation of charm hadron total cross section integrated over momentum space is expected to be less affected by nonperturbative soft processes and hadronization [3]. Systematic studies of charm production in $p + p$ and $p + \text{nucleus}$ collisions have been proposed as a sensitive way to measure the parton distribution function in nucleons, and nuclear shadowing effects [4]. At BNL Relativistic Heavy Ion Collider (RHIC) energies, heavy quark energy loss [5], charm quark coalescence [6–9], possible J/ψ suppression [10], and charm flow [11] have been proposed as important tools in studying the properties of matter created in heavy ion collisions.

Identification of charmed hadrons is difficult due to their short lifetime [$c\tau(D^0) = 124 \mu\text{m}$], low production rates, and large combinatorial background. Most measurements of the total charm cross section in hadron-hadron collisions have been performed at low center-of-mass energies ($\leq 40 \text{ GeV}$) in fixed target experiments [12,13]. At $\sqrt{s} \sim 52\text{--}63 \text{ GeV}$, the available measurements are not conclusive due to inconsistencies between different measurements [12,14]. The measurements at higher energy colliders have been at high p_T only [15] or have included large uncertainties [16,17]. Theoretical predictions for the RHIC energy region differ significantly [18,19]. Therefore, precise measurements of charm cross sections in $p + p$ and $d + \text{Au}$ collisions in this energy region are crucial. In this Letter, we report first results on open charm cross sections at $\sqrt{s_{NN}} = 200 \text{ GeV}$ from direct charmed hadron $D^0(\bar{D}^0)$ reconstruction in $d + \text{Au}$ collisions and from charm semileptonic decay in both $p + p$ and $d + \text{Au}$ collisions. These measurements are complementary, providing important experimental cross-checks.

The data used in D^0 direct reconstruction and charm semileptonic decay analysis were taken during the 2003 RHIC run in $d + \text{Au}$ and $p + p$ collisions at $\sqrt{s_{NN}} = 200 \text{ GeV}$ with the solenoidal tracker at RHIC (STAR). A minimum bias $d + \text{Au}$ collision trigger was defined by requiring at least one spectator neutron in the outgoing Au beam direction depositing energy in a zero degree calorimeter. Detailed descriptions of the trigger and centrality definition in $d + \text{Au}$ collisions have been presented in a previous publication [20]. A total of 15.7×10^6 minimum bias triggered $d + \text{Au}$ collision events were used in the D^0 analysis. The data samples used in the electron analysis in $d + \text{Au}$ and $p + p$ collisions were described

in Ref. [21]. The integrated luminosity is about $40 \mu\text{b}^{-1}$ for $d + \text{Au}$ collisions and 30 nb^{-1} for $p + p$ collisions.

The primary tracking device of the STAR detector is the time projection chamber (TPC) [22]. It was used to reconstruct the decay of $D^0 \rightarrow K^- \pi^+$ ($\bar{D}^0 \rightarrow K^+ \pi^-$) which has a branching ratio of 3.83%. In what follows, we imply $(D^0 + \bar{D}^0)/2$ when using the term D^0 unless otherwise specified. The exact D^0 decay topology cannot be resolved due to insufficient track projection resolution close to the collision vertex. The invariant mass spectrum of D^0 mesons was obtained by pairing each oppositely charged kaon and pion candidate in the same event. The kaon and pion tracks were identified through ionization energy loss (dE/dx) in the TPC wherever the identification is possible. Candidate tracks were selected having momenta p (p_T) > 0.3 (0.2) GeV/c and pseudorapidity $|\eta| < 1$. The D^0 signal with $p_T < 3 \text{ GeV}/c$ and $|y| < 1$ after mixed-event background subtraction [23] is shown in Fig. 1(a). The signal-to-background ratio (S/B) is about 1/600, and the figure of merit (S/\sqrt{B}) is about 6. This distribution was fit to a Gaussian plus a linear function to account for the residual background not described by the mixed-event spectrum [23]. The open symbols in Fig. 1(a) depict the D^0 signal after the two-step background subtraction. HIJING simulations [24] have shown that dihadron correlations from jets can affect the line shape of the background spectrum since the shape (slope versus mass) from this contribution is different from that of random pairs. To estimate the uncertainty in the subtraction of the residual background, different normalizations, slopes, and fit ranges were tried. The resulting uncertainty in the D^0 yield is estimated to be 15%.

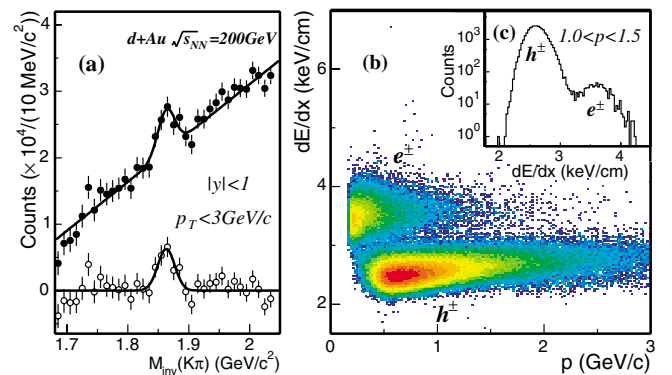


FIG. 1 (color online). (a) Invariant mass distributions of kaon-pion pairs from $d + \text{Au}$ collisions. The solid circles depict the signal after mixed-event background subtraction, the open circles after subtraction of the residual background using a linear parametrization. (b) dE/dx in the TPC versus particle momentum (p) with a TOF cut of $|1/\beta - 1| \leq 0.03$. Inset: projection on the dE/dx axis for particle momenta $1 < p < 1.5 \text{ GeV}/c$.

Within statistical uncertainties, the yields of D^0 and \bar{D}^0 are equal. The $D^0 \rightarrow K^- \pi^+$ signal could be misidentified as a $\bar{D}^0 \rightarrow K^+ \pi^-$ and vice versa when both of its daughters are beyond particle identification in the TPC. This misidentification results in double counting, which was corrected for in the D^0 yields through a Monte Carlo simulation.

Another detector used in this analysis was a prototype time-of-flight system (TOF) [25] based on multigap resistive plate chamber technology. It covers an azimuthal angle $\Delta\phi \simeq \pi/30$, and $-1 < \eta < 0$. In addition to its hadron identification capability [21], it allows electrons/positrons to be identified at low momentum ($p_T < 3$ GeV/c) by using a combination of velocity information (β) from TOF and dE/dx measured in the TPC. Figure 1(b) demonstrates the clean separation of electrons from hadrons using their dE/dx in the TPC after applying a TOF cut of $|1/\beta - 1| \leq 0.03$. This cut eliminated the hadrons crossing the electron dE/dx band. Electrons/positrons were required to originate from the collision vertex. Hadron contamination was evaluated to be about 10%–15% in a selection optimized for purity and statistics. At higher p_T (2–4 GeV/c), electrons could be identified directly in the TPC since hadrons have lower dE/dx due to the relativistic rise of the dE/dx for electrons. Positrons are more difficult to identify using dE/dx alone because of the large background from the deuteron band. The hadron contamination in this case was found to be $\leq 5\%$ at $p_T \simeq 2$ GeV/c and to increase to $\sim 30\%$ at $p_T \simeq 3$ –4 GeV/c. This was corrected for in the final spectra. Detector acceptance and efficiency

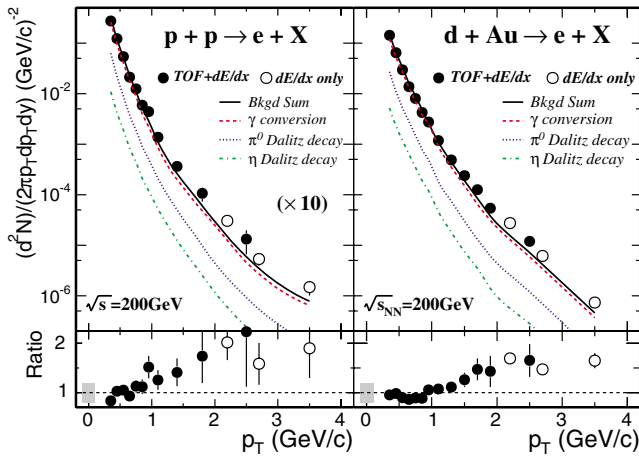


FIG. 2 (color online). Upper panels: Electron distributions from $p + p$ (left) and $d + \text{Au}$ (right) collisions. Solid and open symbols depict electrons/positrons $[(e^+ + e^-)/2]$ identified via a combination of TOF and dE/dx and electrons (e^-) identified via dE/dx alone. The total photonic backgrounds are shown as solid lines. Dashed lines depict the various contributing sources. The fractions were derived from simulations. Bottom panels: The ratio of inclusive electrons to the total backgrounds. The gray band represents the systematic uncertainty in each panel.

corrections were determined from detailed simulations [21]. Total inclusive electron spectra from 200 GeV $p + p$ and collisions are shown in Fig. 2.

Gamma conversions $\gamma \rightarrow e^+e^-$ and $\pi^0 \rightarrow \gamma e^+e^-$ Dalitz decays are the dominant photonic sources of electron background. To measure the background photonic electron spectra, the invariant mass and opening angle of the e^+e^- pairs were constructed from an electron (positron) in TOF and every other positron (electron) candidate reconstructed in the TPC [26]. A secondary vertex at the conversion point was not required. Simulations with both HIJING [24] and PYTHIA [27] with full detector description in GEANT yielded $\sim 60\%$ efficiency for electrons with $p_T > 1$ GeV/c from such background processes. More than 95% of the electrons from sources other than heavy-flavor semi-leptonic decays were measured with this method. The remaining fraction from decays of η , ω , ρ , ϕ , and K was determined from simulations. The results are shown as solid lines in Fig. 2. The overall uncertainty of the background is on the order of 20% and has been included in the systematic errors. Ratios of the inclusive electrons over the total backgrounds are shown in the bottom panels of Fig. 2. The signal is clearly in excess of the background above $p_T > 1$ GeV/c.

The nonphotonic electron spectra were obtained by subtracting the previously described photonic background from the inclusive spectra. The results are shown in Fig. 3. The D^0 invariant yields $d^2N/(2\pi p_T dp_T dy)$ as a function of p_T from direct reconstruction are shown in Fig. 3 as solid squares. Two different fitting methods were used to extract dN/dy for the D^0 at midrapidity. In the first

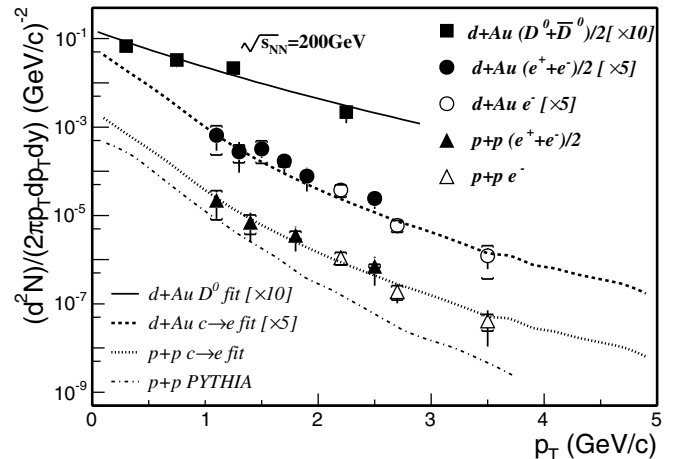


FIG. 3. Reconstructed D^0 (solid squares) p_T distributions from $d + \text{Au}$ collisions at $\sqrt{s_{NN}} = 200$ GeV. Nonphotonic electron p_T distributions from $p + p$ collisions (triangles) and $d + \text{Au}$ collisions (circles). Solid and dashed lines are the fit results from both D^0 and electron spectra in $d + \text{Au}$ collisions. The dotted line is scaled down by a factor of $N_{\text{bin}} = 7.5 \pm 0.4$ [20] from $d + \text{Au}$ to $p + p$ collisions. The dot-dashed line depicts a PYTHIA calculation [27].

TABLE I. dN/dy of D^0 in $d + Au$ collisions and the corresponding $d\sigma/dy$ of $c\bar{c}$ pair per nucleon-nucleon collision at $\sqrt{s_{NN}} = 200$ GeV.

	$dN(D^0)/dy _{y=0}$ (10^{-2})	$d\sigma_{c\bar{c}}^{NN}/dy _{y=0}$ (mb)
D^0	$2.8 \pm 0.4 \pm 0.8$	$0.29 \pm 0.04 \pm 0.08$
$D^0 + e^\pm$	$2.9 \pm 0.4 \pm 0.8$	$0.30 \pm 0.04 \pm 0.09$

method, dN/dy was extracted from an exponential fit to the D^0 differential yield in transverse mass (m_T) [23]. In the second method, a simultaneous fit was applied to both directly reconstructed D^0 's and the background subtracted nonphotonic electron distribution in $d + Au$ collisions. For this fit, it was assumed that the D^0 spectrum follows a power law in p_T from which an electron spectrum was generated using the particle composition from [28] and the decay generators in PYTHIA. A set of parameters for the power law was found at the minimum of χ^2 for the D^0 and electron spectra. The results are shown in Table I. The systematic error is dominated by the uncertainties in the background subtraction, the extrapolation due to finite p_T coverage, and the overall normalization ($\pm 14\%$ in $p + p$ and $\pm 10\%$ in $d + Au$ collisions [20,21]).

The yield of D^0 at midrapidity is $dN/dy = 0.028 \pm 0.004 \pm 0.008$ and the $\langle p_T \rangle = 1.32 \pm 0.08$ GeV/ c in $d + Au$ collisions. We used the ratio $R = N_{D^0}/N_{c\bar{c}} = 0.54 \pm 0.05$ from e^+e^- collider data [28] to convert the D^0 yield to a total $c\bar{c}$ yield. A $p + p$ inelastic scattering cross section of $\sigma_{inel}^{pp} = 42$ mb was used in the calculation, and a factor of $f = 4.7 \pm 0.7$, estimated from simulation [18,27], was used to convert the $d\sigma/dy$ at midrapidity to the total cross section. The total charm cross section per nucleon-nucleon interaction for $d + Au$ collisions at 200 GeV is $\sigma_{c\bar{c}}^{NN} = dN_{D^0}^{d+Au}/dy \times \sigma_{inel}^{pp}/N_{bin}^{d+Au} \times f/R = 1.3 \pm 0.2 \pm 0.4$ mb from D^0 alone and $1.4 \pm 0.2 \pm 0.4$ mb from the combined fit of D^0 and electrons. The nuclear modification factor [20] was obtained by taking the ratio of the electron spectra in $d + Au$ and $p + p$ collisions scaled with the underlying nucleon-nucleon binary collisions. It was measured to be $1.3 \pm 0.3 \pm 0.3$, averaged over $1 < p_T < 4$ GeV/ c . This value is consistent with binary scaling within the measured errors.

The beam energy dependence of the cross section is shown in Fig. 4. Both default PYTHIA [27] and next to leading order (NLO) PQCD [18] calculations reasonably describe the results at lower energies, but underpredict the total charm cross section at $\sqrt{s_{NN}} = 200$ GeV. A NLO PQCD calculation (solid line) with fragmentation and renormalization scales chosen to be $\mu_F = 2m_c$ and $\mu_R = m_c$ ($m_c = 1.2$ GeV/ c^2) reproduces our result. The underprediction by PYTHIA of the charm cross section is also evident in Fig. 3, the charm decayed electron p_T distribution shown as dot-dashed line. Furthermore, the slope of

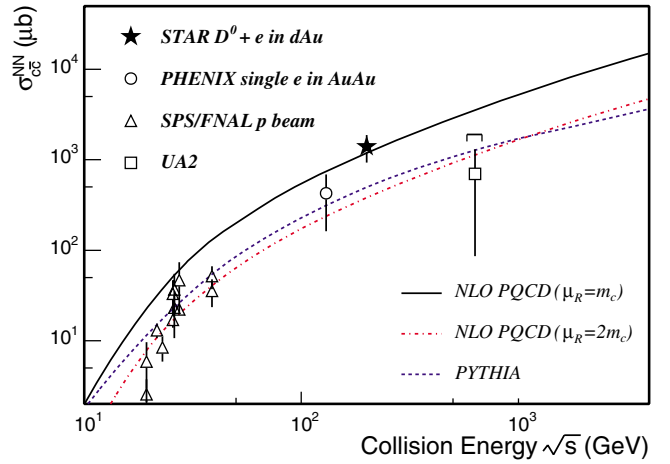


FIG. 4 (color online). Total $c\bar{c}$ cross section per nucleon-nucleon collision versus the collision energy ($\sqrt{s_{NN}}$). The dashed line depicts a PYTHIA calculation [27]. The solid and dot-dashed lines depict two NLO PQCD calculations with the Martin-Roberts-Sterling-Thorne highest order set, $m_c = 1.2$ GeV/ c^2 , $\mu_F = 2m_c$, $\mu_R = m_c$, and $2m_c$, respectively [18].

the PYTHIA distributions is much steeper than the measured distribution. There are also indications that a large charm production cross section at $\sqrt{s_{NN}} \approx 300$ GeV is essential to explain available cosmic ray data [29].

At RHIC energies, binary scaling of the open charm production is expected between $p + p$, $p + A$, and $A + A$ collisions [4]. If correct, the results of this study suggest a much larger charm yield in central Au + Au collisions than previously assumed in statistical thermal models [7–9] based on some PQCD/PYTHIA calculations. This would rule out several predictions [7–9] of charm production not previously excluded by the upper limit (below binary scaling) set by J/ψ production in central Au + Au collisions [30]. Future heavy ion runs at RHIC with open charm and J/ψ measurements will enable us to study the flow and thermalization of charmed particles.

In summary, the charm cross section and transverse momentum distribution for $p + p$ and $d + Au$ collisions at $\sqrt{s_{NN}} = 200$ GeV have been measured by the STAR collaboration at RHIC. Independent measurements of the reconstructed D^0 and single electrons from charm semileptonic decay are consistent. The total cross section at this energy was compared to theoretical calculations. The result has important consequences for charm quark coalescence in Au + Au collisions at RHIC.

We are grateful for many fruitful discussions with D. Kharzeev and R. Vogt. We thank the RHIC Operations Group and RCF at BNL, and the NERSC Center at LBNL for their support. This work was supported in part by the HENP Divisions of the Office of Science of the U.S. DOE; the U.S. NSF; the BMBF of Germany; IN2P3, RA, RPL, and EMN of France; EPSRC of the United Kingdom; FAPESP of Brazil; the Russian Ministry of Science and

Technology; the Ministry of Education and the NNSFC of China; Grant Agency of the Czech Republic; FOM and UU of the Netherlands; DAE, DST, and CSIR of the Government of India; Swiss NSF; and the Polish State Committee for Scientific Research.

-
- [1] P.L. McGaughey *et al.*, Int. J. Mod. Phys. A **10**, 2999 (1995).
- [2] M.L. Mangano *et al.*, Nucl. Phys. **B405**, 507 (1993).
- [3] B.A. Kniehl *et al.*, Nucl. Phys. **B597**, 337 (2001); S. Kretzer, Phys. Rev. D **62**, 054001 (2000).
- [4] Z. Lin and M. Gyulassy, Phys. Rev. Lett. **77**, 1222 (1996).
- [5] Y.L. Dokshitzer and D.E. Kharzeev, Phys. Lett. B **519**, 199 (2001).
- [6] L. Grandchamp and R. Rapp, Phys. Lett. B **523**, 60 (2001).
- [7] A. Andronic *et al.*, Phys. Lett. B **571**, 36 (2003).
- [8] R.L. Thews, M. Schroedter, and J. Rafelski, Phys. Rev. C **63**, 054905 (2001).
- [9] M.I. Gorenstein *et al.*, J. Phys. G **28**, 2151 (2002).
- [10] T. Matsui and H. Satz, Phys. Lett. B **178**, 416 (1986).
- [11] S. Batsouli *et al.*, Phys. Lett. B **557**, 26 (2003); Z. W. Lin and D. Molnar, Phys. Rev. C **68**, 044901 (2003); V. Greco, C. M. Ko, and R. Rapp, Phys. Lett. B **595**, 202 (2004); X. Dong *et al.*, Phys. Lett. B **597**, 328 (2004).
- [12] S. P. K. Tavernier, Rep. Prog. Phys. **50**, 1439 (1987). Total cross sections extrapolated from very high x_F and/or from correlations with low acceptance are not included in Fig. 4.
- [13] E769 Collaboration, G. A. Alves *et al.*, Phys. Rev. Lett. **77**, 2388 (1996).
- [14] F. W. Büsser *et al.*, Nucl. Phys. **B113**, 189 (1976).
- [15] CDF II Collaboration, D. Acosta *et al.*, Phys. Rev. Lett. **91**, 241804 (2003).
- [16] PHENIX Collaboration, K. Adcox *et al.*, Phys. Rev. Lett. **88**, 192303 (2002).
- [17] O. Botner *et al.*, Phys. Lett. B **236**, 488 (1990).
- [18] R. Vogt, Int. J. Mod. Phys. E **12**, 211 (2003); hep-ph/0203151.
- [19] J. Raufeisen and J.-C. Peng, Phys. Rev. D **67**, 054008 (2003).
- [20] STAR Collaboration, J. Adams *et al.*, Phys. Rev. Lett. **91**, 072304 (2003).
- [21] STAR Collaboration, J. Adams *et al.*, nucl-ex/0309012.
- [22] M. Anderson *et al.*, Nucl. Instrum. Methods Phys. Res., Sect. A **499**, 659 (2003).
- [23] STAR Collaboration, C. Adler *et al.*, Phys. Rev. C **66**, 061901(R) (2002); H. Zhang, Ph.D. thesis, Yale University, 2003.
- [24] X.N. Wang and M. Gyulassy, Phys. Rev. D **44**, 3501 (1991).
- [25] B. Bonner *et al.*, Nucl. Instrum. Methods Phys. Res., Sect. A **508**, 181 (2003); M. Shao *et al.*, Nucl. Instrum. Methods Phys. Res., Sect. A **492**, 344 (2002).
- [26] STAR Collaboration, J. Adams *et al.*, Phys. Rev. C **70**, 044902 (2004); I. Johnson, Ph.D. thesis, University of California, Davis, 2002.
- [27] T. Sjöstrand *et al.*, Comput. Phys. Commun. **135**, 238 (2001). PYTHIA 6.152 was used with the parameter settings: MSEL = 1, CTEQ5M1. Bottom contribution was estimated to be 20%–30% in $p_T = 2\text{--}3$ GeV/ c , 40%–50% in 3–4 GeV/ c to the total nonphotonic electrons, and negligible at lower p_T .
- [28] Particle Data Group, K. Hagiwara *et al.*, Phys. Rev. D **66**, 010001 (2002). $N_{D^0}/N_{c\bar{c}}$ was derived from the measured open charm states in e^+e^- at $\sqrt{s} = 91$ GeV. There is a 10% uncertainty taken into account in the branching ratios of open charm semileptonic decays used in the electron-to-charm fit, reflecting unknown production and branching ratios for individual states. The ratio in hadronic production, although somewhat reduced, is consistent with that in e^+e^- within errors.
- [29] I. V. Rakobolskaya *et al.*, Nucl. Phys. (Proc. Suppl.) **B122**, 353 (2003).
- [30] PHENIX Collaboration, S. S. Adler *et al.*, Phys. Rev. C **69**, 014901 (2004); PHENIX Collaboration, S. S. Adler *et al.*, Phys. Rev. Lett. **92**, 051802 (2004).